Astronomy & Astrophysics manuscript no. gd1_mepp
September 26, 2023

Modelling the formation of the GD-1 stellar stream inside a host with a fermionic dark matter core-halo distribution.

Martín F. Mestre[1,2,⋆], Carlos R. Argüelles[1,2], and Daniel D. Carpintero[1,2]

[1] Instituto de Astrofísica de La Plata (CONICET-UNLP), Paseo del Bosque S/N, La Plata (1900), Buenos Aires, Argentina

[2] Facultad de Ciencias Astronómicas y Geofísicas de La Plata (UNLP), Paseo del Bosque S/N, La Plata (1900), Buenos Aires, Argentina

Received February 30, 2023; accepted February 31, 2023

ABSTRACT

Context. Stellar streams are a consequence of the tidal forces produced by a host galaxy on its satellites (i.e. globular clusters and dwarf spheroidals). As the self-gravity of stellar streams is almost negligible, they constitute excellent probes of the gravitational potential of the host galaxy. For this reason, some Milky Way stellar streams have been used to put constraints on the dark matter (DM) total mass and shape, under empirical DM distributions (i.e. NFW, logarithmic, etc). Within the set of non-empirical DM distributions, there exists a DM model deduced from first principles by means of the maximization of the coarse-grained entropy for self-gravitating fermions, the MEPP, after Maximum Entropy Production Principle. MEPP profiles have a rich variety of behaviours, being a large subfamily characterized by a dense core of mass $\approx 4.1 \times 10^6 M_\odot$ (that can mimick a black hole regarding the orbits of the S-stars at Sagittario A*) and an extended halo with the plasticity of a Burkert profile.
Aims. In this work we attempt to model the GD-1 stellar stream using a spherical MEPP distribution which, at the same time, is in sintony with previous fits to the S-stars.
Methods. For that purpose we used a genetic algorithm in order to fit both the stream orbit's initial conditions and the fermionic halo. We modelled the barionic potential with a bulge and two disks (thin and thick) with fixed parameters according to the recent literature. The stream observable is 6D phase-space data from the Gaia DR2 survey.
Results. We were able to find good fits for a 1D continuous subfamily of models parametrized by the fermion mass going from 56 keV/c^2 to 360 keV/c^2, respectively corresponding to core radii going from 10^3 to 10 Schwarzschild radii. For smaller and larger values of the fermion mass, there is no solution that simultaneously fits the GD-1 stream and the S-stars. The solutions have a virial radius of 28 kpc and a virial mass of $1.4 \times 10^{11} M_\odot$, the latter being at 2σ from previous Milky Way DM halo mass estimates using the Sagittarius stream. We do not assume the velocity of the local standard of rest ($v_{\rm lsr}$) and the result gives $v_{\rm lsr} \approx 244$ km/s, in agreement with recent independent estimates.

Key words. Galaxy: kinematics and dynamics – Galaxy: stellar streams – dark matter

1. Introduction

When a galaxy hosts a satellite, i.e. dwarf galaxy or globular cluster, the gravitional interaction between them modifies both subsystems. The host galaxy strips stars from the satellite at a rate that depends on their density profiles and on the orbit, while the host density profile suffers a reorganization of its matter in the vecinity of the satellite's orbit, developing a wake due to the dynamical friction. This ensemble of stars tidally stripped from the satellite constitute a stellar stream (also named tidal stream) and examples of them have been detected in the Milky Way (MW) and in Andromeda, with different observational techniques.

At present stellar streams constitute one of the main MW observables related to the dynamics, together with other baryonic observables like the rotation curve, the radial surface density profile of the disk and the vertical density profile of the disk at the solar radius. Tidal streams probe the acceleration field produced by the Galaxy (Johnston et al. 1999; Zhao et al. 1999; Law et al. 2009; Lux et al. 2013; Johnston & Carlberg 2016; Ibata et al. 2016; Ibata et al. 2017; Thomas et al. 2017; Reino et al. 2021) as well as its formation history according to Helmi et al. (1999); Helmi (2020); Ramos et al. (2022); Cunningham et al. (2023) among others. *A stellar stream could be the closest realization of a galactic orbit that can be observed in nature*. Nevertheless, the larger the progenitor, the more discrepancy between its orbit and the stream phase-space configuration. In fact, the taxonomy of streams is very rich (Amorisco 2015) because of the different gravitational configurations that can take place, going from almost unidimensional streams whose progenitor is a small globular cluster to a wide shell produced by the partially radial sinking into the MW centre of a large progenitor. Besides, it is theoretically possible to have accreted streams, whose progenitor is a globular cluster orbiting a MW's satellite galaxy, giving place to stellar cocoons around the stream tracks as studied by Carlberg (2018); Malhan et al. (2019, 2021); Gialluca et al. (2021); Qian et al. (2022).

Stream data together with other baryonic measurements can help in making claims about unknown aspects of the gravitational field: model either a dark matter (DM) halo component or a modified Newtonian dynamics (MOND) theory. For example, within the DM paradigm, a given candidate to the DM particle

⋆ e-mail: mmestre@fcaglp.unlp.edu.ar

corresponds to certain family of halo and subhalo phase-space distributions, which in turn, are responsible for the satellite orbit and the phase-space density distribution of the stream. Besides, DM space densities might have different shapes (e.g. spherical, axisymmetric, triaxial) depending on the number of conserved components of the angular momentum, which also incluences the stream properties as discussed in Vera-Ciro & Helmi (2013); Price-Whelan et al. (2016); Mestre et al. (2020). In particular, Malhan & Ibata (2019) have constrained the MW dark matter halo shape using Gaia DR2 data of the the GD-1 stream, assuming a triaxial generalization of the NFW profile and obtaining a flattening halo parameter of $q = 0.82^{+0.25}_{-0.13}$, thus compatible with a situation of spherical symmetry. Moreover, (Palau & Miralda-Escudé 2023) has measured the oblateness in an axisymmetric generalization of the NFW profile using three stellar streams: NGC 3201, M68 and Palomar 5.

Por favor Charly agrega desde aca... In the recent literature many types of DM candidates have been analyzed, like axions, bosons and fermions. In this work we will work with the relativistic fermionic King model defined in Chavanis (2020), as implemented in the RAR model (Argüelles et al. 2018). ...hasta aca.

In this paper we will model the formation of the GD-1 stellar stream inside a MW with a relativistic fermionic King dark matter core-halo distribution. In Sec. 2 we explain the work methodology. In Sec. 3 we present the results and in Sec. 4 we give the conclusions.

2. Methodology

In this section we explain the observables and methods used in this research. The exact pipeline applied in order to obtain the results and plots of this paper can be found at the following GitHub repository: https://github.com/martinmestre/stream-fit/blob/main/pipeline_paper/.

2.1. Observables and assumed measurements

The main observables used in this project are materialized by the polynomial fits performed by Ibata et al. (2020) on the GD-1 stream using astrometry (Gaia DR2), photometry and high-precision spectroscopy datasets together with the analysis of the STREAMFINDER algorithm. Those polinomials are the following:

$$\phi_2 = 0.008367\phi_1^3 - 0.05332\phi_1^2 - 0.07739\phi_1 - 0.02007, \quad (1)$$

$$D = -4.302\phi_1^5 - 11.54\phi_1^4 - 7.161\phi_1^3 + 5.985\phi_1^2 + 8.595\phi_1 + 10.36, \quad (2)$$

$$\tilde{\mu}_\alpha = 3.794\phi_1^3 + 9.467\phi_1^2 + 1.615\phi_1 - 7.844, \quad (3)$$

$$\mu_\delta = -1.225\phi_1^3 + 8.313\phi_1^2 + 18.68\phi_1 - 3.95, \quad (4)$$

$$v_h = 90.68\phi_1^3 + 204.5\phi_1^2 - 254.2\phi_1 - 261.5, \quad (5)$$

(6)

with ϕ_1 and ϕ_2 in radians, D in kpc, $\tilde{\mu}_\alpha = \mu_\alpha cos\delta$ and μ_δ in mas/yr and v_h in km/s. These quantities correspond respectively to longitude and latitude in GD-1 celestial frame of reference (Koposov et al. 2010), heliocentric distance, proper motion in right ascension and declination, and heliocentric radial velocity. The domain of this polinomials is limited to $-90 < \phi_1[^\circ] < 10$. To have our observable data points we sample the domain with 100 points ($\phi_1^{(i)}$ for $i = 1, ..., 100$) and evaluate the polinomials there in order to have a complete set of observables ($\phi_1^{(i)}$, $\phi_2^{(i)}, D^{(i)}, \tilde{\mu}_\alpha^{(i)}, \mu_\delta^{(i)}, v_h^{(i)}$). In one of the experiments we will consider an observable of a different nature and related to the density concentration at the origin, of size $\lesssim 1$ milliparsec, characteristic of the fermionic halo distribution. By convention, the core radius is defined as the radius when the circular velocity reaches its first maximum. The constraint for the mass of the core of the distribution is assumed to be $m_{\rm core} = 3.5 \times 10^6 M_\odot$ in agreement with Becerra-Vergara et al. (2020, 2021); Argüelles et al. (2022).

The assumed measurements used in this paper are the galactocentric distance of the sun $R_\odot = 8.122$ kpc (GRAVITY Collaboration et al. 2018) and the sun's peculiar velocity $\boldsymbol{v}_{\odot p} = (11.1, 12.24, 7.25)$ km/s (Schönrich et al. 2010).

2.2. The relativistic fermionic King DM model

Our DM model consists of the relativistic fermionic King model (here denoted just "fermionic") which is a spherical and isotropic distribution of fermions at finite temperature in hydrostatic equilibrium subject to the law of General Relativity (GR), i.e. T.O.V equations, as defined in Argüelles et al. (2018) with the particularity that we have made a few change of variables in order to make the numerical computation more robust. The system of equations thus obtained is as follows:

$$\frac{d\nu}{d\zeta} = \frac{1}{2}\left[e^z + e^{2\zeta}\frac{P(r)}{\rho_{rel}c^2}\right][1 - e^z]^{-1}, \quad (7)$$

$$\frac{dz}{d\zeta} = -1 + e^{(2\zeta - z)}\frac{\rho(r)}{\rho_{rel}}, \quad (8)$$

where

$$\zeta = \ln(r/R), \quad (9)$$

$$z = \ln\psi, \quad \psi = \frac{M_{\rm DM}(r)}{M}\frac{R}{r}, \quad (10)$$

$$\rho(r) = \frac{4\rho_{\rm rel}}{\sqrt{\pi}}\int_1^\infty \epsilon^2[\epsilon^2 - 1]^{1/2} f(r,\epsilon)d\epsilon, \quad (11)$$

$$P(r) = \frac{4\rho_{\rm rel}c^2}{3\sqrt{\pi}}\int_1^\infty [\epsilon^2 - 1]^{3/2} f(r,\epsilon)d\epsilon, \quad (12)$$

$$R^2 = \frac{c^2}{8\pi G\rho_{\rm rel}}, \quad (13)$$

$$M = 4\pi R^3 \rho_{\rm rel}, \quad (14)$$

$$\rho_{\rm rel} = \frac{G\pi^{3/2}m^4c^3}{h^3}, \quad (15)$$

where G is the Gravitational constant, c is the speed of light, h is the Planck constant, m is the fermion mass, $M_{\rm DM}(r)$ is DM mass enclosed up to radius r, $\rho(r)$ is the density, $P(r)$ is the pressure and $\nu(r)$ is the metric exponent, i.e. we use the convention $g_{00} = e^{\nu(r)}$. The phase-space function (f) is given by a Fermi-Dirac distribution with energy cutoff:

$$f(r,\epsilon) = \begin{cases} \dfrac{1 - e^{[\epsilon - \epsilon_c(r)]/\beta(r)}}{1 + e^{[\epsilon - \alpha(r)]/\beta(r)}} & \epsilon \le \epsilon_c(r) \\ 0 \quad \epsilon > \epsilon_c(r), \end{cases} \quad (16)$$

where $\alpha(r)$ is the chemical potential (including rest mass), $\epsilon_c(r)$ is the cutoff energy (including rest mass) and $\beta(r)$ is the temperature variable.

The above equations should be complemented with two thermodinamic equilibrium conditions given in Tolman (1930) and Klein (1949) together with the condition of energy conservation along the geodesic given in Merafina & Ruffini (1989):

$$\frac{1}{\alpha}\frac{d\alpha}{dr} = \frac{1}{\beta}\frac{d\beta}{dr} = \frac{1}{\epsilon_c}\frac{d\epsilon_c}{dr} = -\frac{1}{2}\frac{d\nu}{dr}. \quad (17)$$

It is not possible to integrate this equations from $r = 0$ because the right hand the change of variables $\zeta(r)$ is divergent at the origin. Nevertheless, it is possible to reach the following approximations for the initial conditions at a value $r_{\rm min} \gtrsim 0$:

$$\nu(r_{\rm min}) \approx \frac{1}{6}\frac{\rho_0}{\rho_{\rm rel}}\left[\frac{r_{\rm min}}{R}\right]^2 \equiv \tau, \quad (18)$$

$$\psi(r_{\rm min}) \approx \frac{1}{3}\frac{\rho_0}{\rho_{\rm rel}}\left[\frac{r_{\rm min}}{R}\right]^2 = 2\tau, \quad (19)$$

which implies

$$\frac{r_{\rm min}}{R} = \sqrt{6\tau\frac{\rho_{\rm rel}}{\rho_0}}, \quad (20)$$

where $\rho_0 \equiv \rho(0)$. It can be seen that the right hand side of Eq. 7 does not depend on the metric so we can add a constant ν_0 to the solution in order to satisfy a condition of continuity with the Schwarzschild metric at the border of the fermion distribution, obtaining:

$$\nu_0 = 2\ln\left(\frac{\beta_b}{\beta_0}\sqrt{1-\psi_b}\right),$$

where ψ_b and β_b are quantities evaluated at the border.

The system of equations thus obtained has four free parameters: m, $\alpha_0 = \alpha(0)$, $\beta_0 = \beta(0)$, and $\epsilon_{c0} = \epsilon_c(0)$ but in practice we will use the following related quantities as parameters: m, β_0, $\theta_0 = (\alpha_0 - 1)/\beta_0$, and $W_0 = (\epsilon_{c0} - 1)/\beta_0$.

Equations 7-17 are solved using a Python (Van Rossum & Drake Jr 1995) script[1] that makes use of the *NumPy* (Virtanen et al. 2020) and *SciPy* (Harris et al. 2020) libraries. We tried all the solvers available in the latter package but the only one that could properly integrate these equations was the `LSODA` algorithm. We used relative and absolute tolerance parameters respectively given by `rtol`= 5×10^{-14} and `atol`= 0.

2.3. Milky Way and stream models

We model our Galaxy with a combination of the fermionic dark halo recently described, whose parameters will be determined in this work, plus a barionic component fixed and identical to the one in Model I of Pouliasis et al. (2017). Here we name this full Galaxy model as Fermionic-MW.

Appart from our model, for some intermediary tasks, we will make use of the Galactic model fitted by Malhan & Ibata (2019) which consists in the `MWPotential2014` model with an axisymmetric NFW profile. This fitted model corresponds to a circular velocity at the position of the sun of $v_c(R_\odot) = 244 \pm 4 {\rm kms}^{-1}$ and a $z-$flattening of the DM density distribution of $q_\rho = 0.82^{+0.25}_{-0.13}$. Here we name this Galaxy model as NFW-MW.

As GD-1 is a dynamically cold stream, with its stars keeping a large degree of correlation, its almost one-dimensional distribution in phase-space can be well approximated with the orbit of its progenitor. Another facts in this direction, are that there has not been any observation of the tidal arms feature nor of the progenitor's position (Malhan & Ibata 2019; de Boer et al. 2018; Malhan et al. 2018; Price-Whelan & Bonaca 2018).

In the code, the orbit model is computed starting from initial conditions in spherical equatorial coordinates, ICRS frame: α (RA), δ (declination), $D, \tilde{\mu}_\alpha, \mu_\delta, v_h$. The code uses the *Astropy* ecosystem (Astropy Collaboration et al. 2022, 2018, 2013) in order to transform the initial condition to galactocentric coordinates assuming a Galactocentric reference frame with the sun at the position $\boldsymbol{x}_\odot = (-R_\odot, 0, 0)$ and a sun's velocity given by the sum of the circular velocity at the position of the sun and the sun's peculiar velocity: $\boldsymbol{v}_\odot = (11.1, v_c(R_\odot) + 12.24, 7.25)$. The circular velocity is dependent on the model and the position and given by

$$\begin{aligned} v_c^2(R_\odot) &= R_\odot \|\nabla\Phi(\boldsymbol{x})\|_{\boldsymbol{x}=\boldsymbol{x}_\odot} \\ &= R_\odot \|\nabla\Phi_{\rm B}(\boldsymbol{x})\|_{\boldsymbol{x}=\boldsymbol{x}_\odot} + G\frac{M_{\rm DM}(R_\odot)}{R_\odot}, \end{aligned} \quad (21)$$

where Φ is the total potential, Φ_B is the potential generated by the three barionic components and $M_{\rm DM}(r)$ was defined in Eq. (10). We have used the spherical symmetry property of the DM distribution in order to relate the acceleration with the enclosed mass.

A second step is to integrate the orbit forwards and backwards in time during a time interval of $\Delta t = 0.2$ Gyr, starting in both cases from a given initial condition for the progenitor. In the next sections we will explain how this initial condition was chosen for some simulations and fitted for others. The integrator used is a Runge-Kutta of order eight (`DOP853` called from *SciPy*'s `solve_ivp` function) with relative and absolute tolerance parameters respectively given by `rtol`= 5×10^{-14} and `atol`= 0.5×10^{-14}.

After having the stream's orbit integrated, we transform the orbit to both the ICRS and the GD-1 frame of coordinates. For the latter we used the `GD1Koposov10` class defined in the Gala package (Price-Whelan 2017; Price-Whelan et al. 2020) which uses the transformation matrix defined by Koposov et al. (2010). After these two transformation we obtain the orbit expressed in the observable variables $(\phi_1, \phi_2, D, \tilde{\mu}_\alpha, \mu_\delta, v_h)$ used in Eqs. (1)-(6). Finally, we build interpolators of these variables as a function of ϕ_1 that will be used, together with the observed data defined in Sec. 2.1, to evaluate the following χ^2 stream function:

$$\chi^2_{\rm stream} = \chi^2_{\phi_2} + \chi^2_D + \chi^2_{\tilde{\mu}_\alpha} + \chi^2_{\mu_\delta} + \chi^2_{v_h}, \quad (22)$$

$$\chi^2_\eta = \frac{1}{\sigma^2_\eta}\sum_{i=1}^{100}\left(\eta^{(i)} - \eta(\phi_1^{(i)})\right)^2, \quad (23)$$

where η represents each of the four corresponding independent variables $(\phi_2, D, v_h, \tilde{\mu}_\alpha, \mu_\delta)$ and σ_η is the average dispersion of the stream data points taken by ocular inspection from Figs. 1,3,4 of Ibata et al. (2020): $\sigma_{\phi_2} = 0.5°$, $\sigma_D = 1.5$ kpc, $\sigma_{v_h} = 10$ km/s and $\sigma_{\tilde{\mu}_\alpha} = \sigma_\delta = 2$ mas/yr. Thus $\chi^2_{\rm stream}$ measures the departure of the model from the stream observations. For some fits we will also consider the departure of the model from a dark mass constraint in the core of the distribution:

$$\chi^2_{\rm core} = \frac{(m_c - m_{\rm core})^2}{\sigma^2_m}, \quad (24)$$

where $m_{\rm core}$ was defined in Sec. 2.1, m_c is the core mass of the model, and σ_m was fixed in 1% of $m_{\rm core}$, so sometimes we will use the following compound function:

$$\chi^2_{\rm full} = \chi^2_{\rm stream} + \chi^2_{\rm core}. \quad (25)$$

Note that in order to compute the estimated core mass of each model, m in Eq.(24), we must find the first local maximum of the expression for the circular velocity in GR:

$$v_{\rm DM}(r) = c\sqrt{\frac{r}{2}\frac{d\nu(r)}{dr}}. \quad (26)$$

[1] `model_def.py`

2.4. Optimization algorithms

Our objective consists in fitting our MW model by minimizing the χ^2 function given by Eqs. (22,25). In order to do so we use two optimization algorithms for different purposes that will be explained in Sec. 3. One of them is *SciPy*'s `optimize.differential_evolution` algorithm. This genetic architecture was used with metaparemeters given by `strategy="best2bin"`, `maxiter`=200, `popsize`=200, `tol`=5×10^{-8} and `atol`=0, unless otherwise stated. This method can be run in parallel with shared memory, so a convergence test was made in a cluster's node with 64 logical processors, varying the values of the metaparameters (e.g. halving and doubling the values of `maxiter` and `popsize`, setting `strategy="best1bin"` and combinations).

The other algorithm is an implementation of the Mesh Adaptive Direct Search algorithm called `NOMAD` (Audet et al. 2021). The Julia (Bezanson et al. 2017) wrapper of this algorithm, *NOMAD.jl*, is used through the package *Optimization.jl*. We used default values of all the metaparameters except for `maxiters`=700.

3. Results

3.1. Fitting the Fermionic-MW model

In this section we will fit both the Fermionic-MW model parameters and the initial condition (IC) of the progenitor orbit through a series of steps. Initially, we searched for a (transitory) good enough IC of the progenitor orbit for our Fermionic-MW. For that, we fitted the initial conditions in the (fixed) NFW-MW model defined in Sec. 2.3 by using the $\chi^2_{\rm stream}$ function defined in Eq. (22) and the genetic algorithm specified in Sec. 2.4. The genetic algorithm needs to be provided with bounds for the variables so we used boxes with a centre close to the middle point of the observable data, i.e. $\eta^{(51)}$ that corresponds to $\alpha = 149.24°$, $\delta = 36.61°$, $D = 7.69$ kpc, $\tilde{\mu}_\alpha = -5.70$ mas/yr, $\mu_\delta = -12.48$ mas/yr and $v_h = -18.81$ km/s, and with generous sides of length equal to their absolute values (except for α where we used a side of lenght $\alpha/5$).

It should be said that the NFW-MW model was fitted by Malhan & Ibata (2019) with a set of Gaia DR2 data different from the polynomials used here. Any point along the stream is equally good as an IC. The genetic algorithm converged to a solution given approximately by $\alpha = 149.17°$, $\delta = 36.51°$, $D = 7.95$ kpc, $\tilde{\mu}_\alpha = -6.94$ mas/yr, $\mu_\delta = -12.49$ mas/yr and $v_h = -18.33$ km/s with a value of $\chi^2_{\rm stream} \approx 17.52$. The orbit that corresponds to this IC is displayed in the observable space in Fig. 1 (top: ϕ_2, middle: $\tilde{\mu}_\alpha$, bottom: μ_δ) and Fig. 2 (top: D, bottom: v_h) with a dotted (green) line. The solid (black) line shows the corresponding observable η data while the shaded (grey) area demarkates the corresponding $1\sigma_\eta$ regions.

From previous works (Argüelles et al. 2018; Argüelles et al. 2019; Krut et al. 2023) we know that the fermionic DM model parameters can be approximately grouped in two sets with different functionality. One group is formed by ϵ and β_0 that control the core of the distribution in the sense that for given values of $m_{\rm core}$ (Sec. 2.1) and ϵ, it is possible to find a value of β_0 in agreement; with a very small influence of the other two parameters: θ_0 and W_0. This implies a partial degeneracy between ϵ and β_0. The other group is formed by θ_0 and W_0, which have small effect on the core region but determine the distribution behaviour in the halo region. Additionally, there is also an approximate degeneracy between these two variables in the sense that it is the parameter $\omega_0 = W_0 - \theta_0$ which mainly controls the halo profile, as will be further shown in this paper.

As a starting point for the parameter fit, we took the result from Becerra-Vergara et al. (2020) who found that for $(\epsilon, \beta_0, \theta_0, W_0) = (56, 1.1977\times10^{-5}, 37.765, 66.3407)$ their MW model (DM+barions) satisfies both the geodesic motion of S2 and G2 at Sagittarius A*, i.e. $m_{\rm core} = 3.5\times10^5 M_\odot$, and the rotation curve from Sofue (2013). As a first step, we fixed values for $\epsilon = 56$ and fixed the IC that was recently fitted for the NFW-MW model, in order to perform a genetic minimization of the $\chi^2_{\rm full}$ function in the window: $(\theta_0, \omega_0, \beta_0) \in [35, 40] \times [25, 30] \times [10^{-5}, 1.5\times10^{-5}]$. Using metaparameter values `maxiter=popsize`=400, the algorithm converged to $(\theta_0, \omega_0, \beta_0) \approx (36.0665, 27.3471, 1.25713\times10^{-5})$ with a value of $\chi^2_{\rm stream} \approx 21.9585$ and $\chi^2_{\rm core} \approx 1.117$. Although the stream fit is good (as will later be shown), the associated value of the core mass was $m_c \approx 3.537\times10^6 M_\odot$ which implies that there is room for improvement. We took this result to shrink the window to $(\theta_0, \omega_0, \beta_0) \in [35, 37] \times [26, 28] \times [1.2\times10^{-5}, 1.3\times10^{-5}]$ and re-run the genetic algorith, converging to $(\theta_0, \omega_0, \beta_0) \approx (36.0661, 27.3468, 1.25769\times10^{-5})$ with a value of $\chi^2_{\rm stream} \approx 21.9585$ and $\chi^2_{\rm core} \approx 1.344\times10^{-5}$ which corresponds to a much precise value of the core mass, $m_c \approx 3.5001\times10^6 M_\odot$. It can be noticed the great sensitivity of the core mass depence on the model parameters because a change in the fifth significant digit of the parameters propagates to a change of in the third significant digit of m_c. Nevertheless, both solutions above are astrophysically equivalent because Becerra-Vergara et al. (2021) has prooved that core masses in the range $[3.5, 3.55]\times10^6 M_\odot$ give good fits of the S-stars.

The last step consisted in fixing the Fermionic-MW parameters while floating the ICs of the orbit with the genetic scheme, with metaparameter values `maxiter=popsize`=400, which gave us very similar to the FMW-MW case: $\alpha = 149.21°$, $\delta = 36.69°$, $D = 7.95$ kpc, $\tilde{\mu}_\alpha = -6.94$ mas/yr, $\mu_\delta = -12.45$ mas/yr and $v_h = -19.15$ km/s, with an improved value of $\chi^2_{\rm stream} \approx 19.32$. The corresponding orbit is displayed in the observable space in Figs. 1-2 with a dashed (amber) line where it can be noticed that both the Fermionic-MW and NFW-MW models fit the GD-1 stream very well. We have not performed any statistically rigourous comparison between both models to determine which one is more consistent with the data. In fact, here we used a fixed NFW-MW model that was fitted by Malhan & Ibata (2019) with another set of Gaia DR2 observations, as has previously been stated.

We would like to give a glimpse of the behaviour of the $\chi^2_{\rm stream}$ function so we have evaluated it for fixed values of $(\epsilon, \beta_0) = (56, 1.258\times10^{-5})$ in a bidimensional grid spanning the box $(\theta_0, \omega_0) \in [34, 38] \times [25, 30]$. Fig. 3 shows a contourplot of this grid coloured by the value of their corresponding $\chi^2_{\rm stream}$ and the black point corresponds to our fitted solution. It can be noticed that the minimum values of the function are located along a thin and finite *valley*, implying that the solution of the fitting problem is locally degenerate along a straight line in the (θ_0, ω_0)-plane. In spite of this, it was possible to fit the Fermionic-MW model with a quality as good as in the NFW-MW model. As an additional check, we have fitted a line to those points that satisfy $\chi^2_{\rm stream} < 50$ obtaining $h(x) \approx 0.7989 + 0.7361x$, substracted this line to ω_0 and made a plot of $\chi^2_{\rm stream}$ function for $(\epsilon, \beta_0) = (56, 1.258\times10^{-5})$ in the window $(\theta_0, \omega_0 - h(\theta_0)) \in [35, 37] \times [-0.011, 0.011]$. The result can be seen in the contour

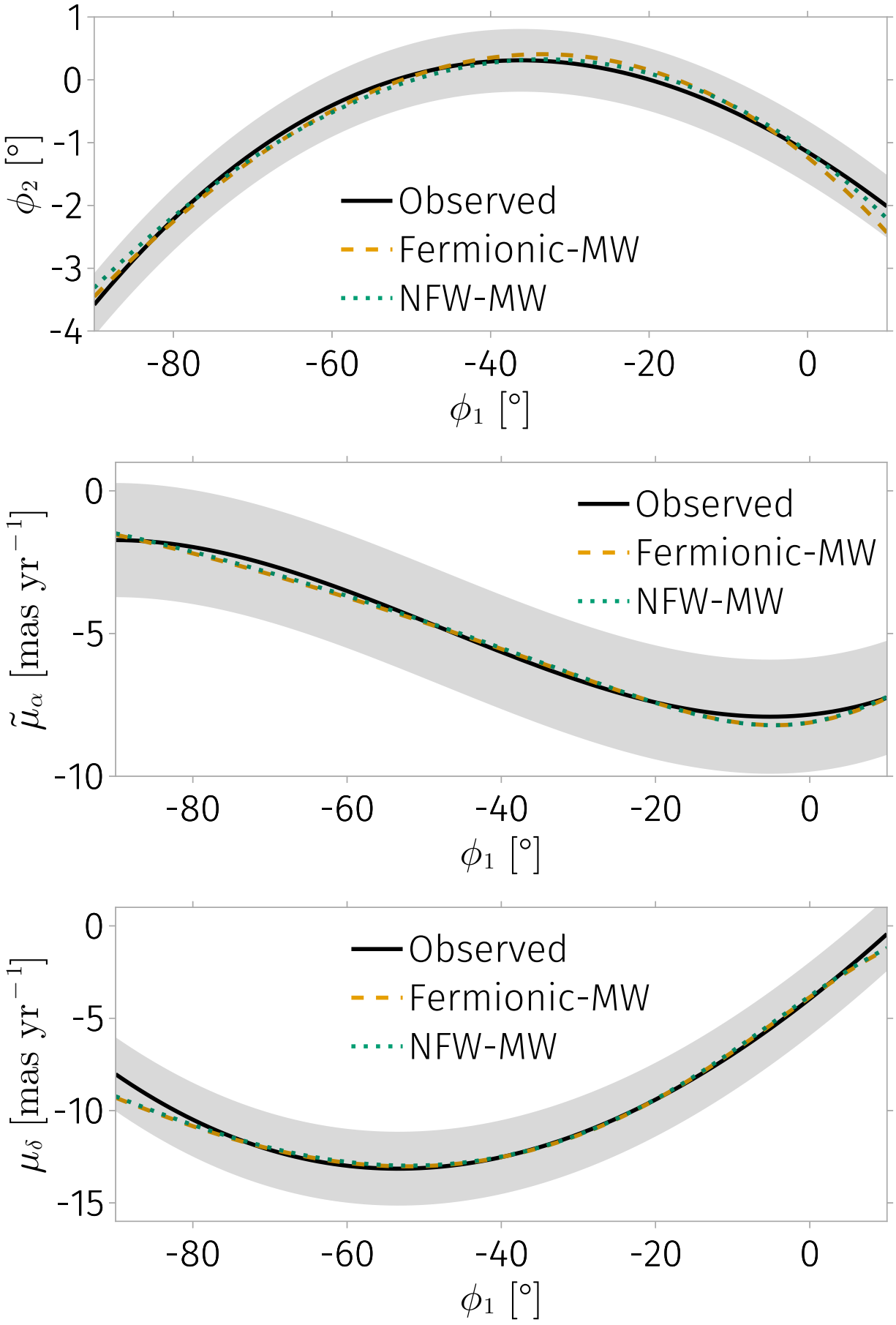

Fig. 1. Stream fits in astrometric observable space: sky position (top: ϕ_2) and proper motions (middle: $\tilde{\mu}_\alpha$, bottom: μ_δ).

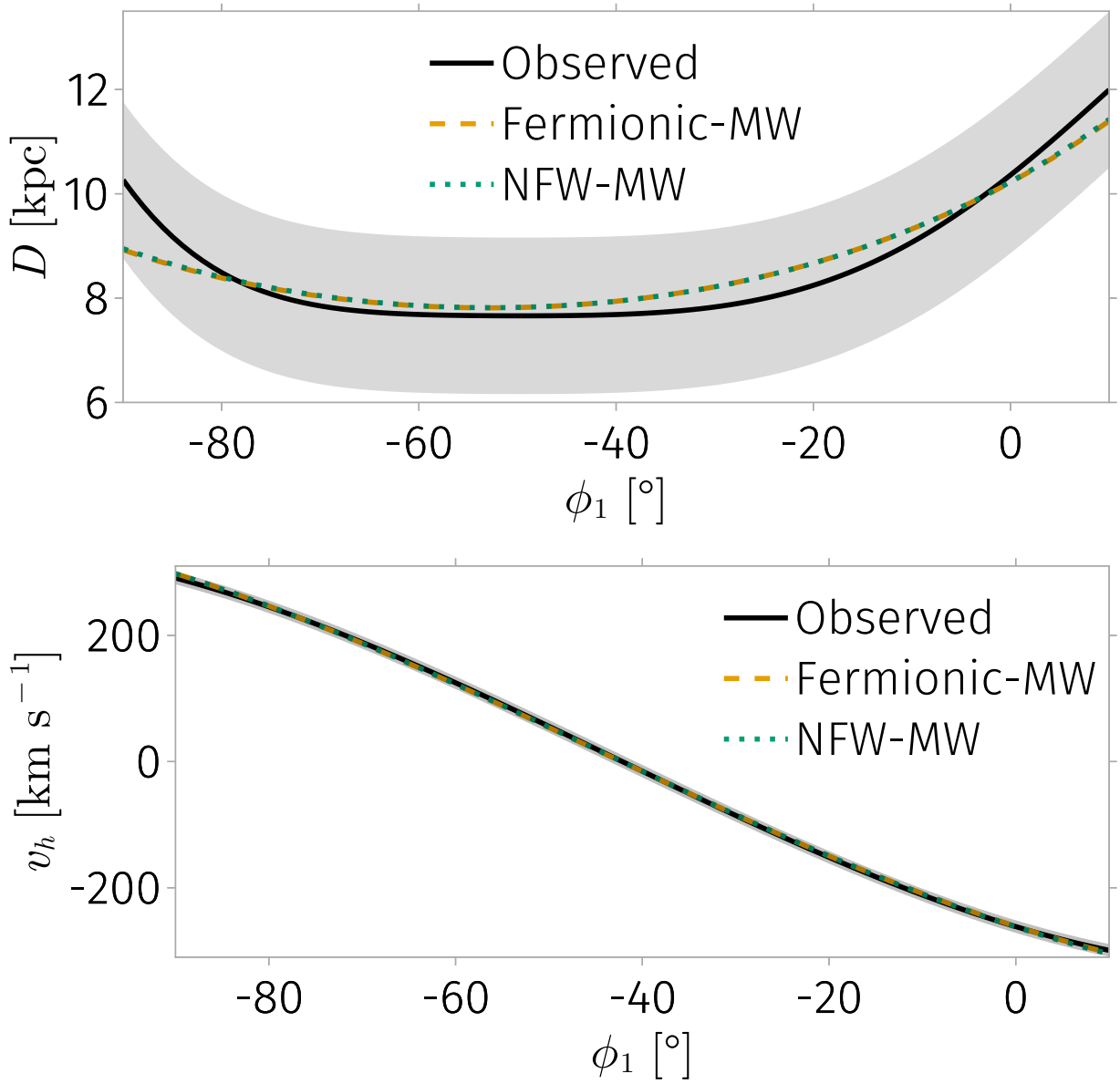

Fig. 2. Stream fits in observable space: photometric distance (top: D) and spectroscopic heliocentric velocity (bottom: v_h).

plot of Fig. 4. It is noticeable that the variance along $\omega_0 - h(\theta_0)$ is two orders of magnitude smaller than the variance along θ_0.

3.2. Rotation curves and virial quantities

As a way to compare our stream results with a more classical MW observable, we have compute the rotation curves for both models and plot them together with three independent rotation curve observations in Fig. 5. For the MW models we have used the same linestyles and colours that were used in previous figures: dotted (green) for the NFW-MW and dashed (amber) for the Fermionic-MW. The rotation curve data is given according to the following marker styles: squares (magenta) for Sofue (2013), circles (blue) for Eilers et al. (2019) and rhombus (light-blue) for Sofue (2020). Note that for building this rotation observables Sofue (2013) assumes a value of $(R_\odot, v_c(R_\odot))$=(8 kpc, 200 km/s) and Sofue (2020) assumes a value of $(R_\odot, v_c(R_\odot))$=(8 kpc, 238 km/s), while Eilers et al. (2019) assumes $R_\odot = 8.122$ kpc and a Galactocentric sun velocity $v_\odot = (11.1, 245.8, 7.8)$ km/s, in order to estimate a value of $v_c(R_\odot) = 229 \pm 0.2$ km/s.

According to GD-1 observables, the present Galactocentric distance projected onto the plane $z = 0$, belongs to the interval $11.5 \lesssim D_g \lesssim 16.4$ (kpc), displayed as a vertical shaded (grey) band in Fig. 5. Although the GD-1 stream orbit location corresponds to $z \in [2.6, 9.7]$ kpc and thus explores the non-sphericality of the full MW models (due to baryons/NFW axisymmetry), the fact that both models approximately agree in their circular velocity values in the GD-1 region gives support to the idea of using stellar streams as Galactic accelerometers (Ibata et al. 2016; Nibauer et al. 2022; Craig et al. 2023). It is interesting to note a coincidence between both models in their values of circular velocity at the position of the sun as they both give a value of $v_c(R_\odot) \approx 244$ km/s. Besides, this values are in perfect agreement with the independent estimate found by Bovy (2020), which are $v_c(R_\odot) = 244 \pm 8$ km/s for $R_\odot \approx 8.275$ kpc, or $v_c(R_\odot) = 242 \pm 8$ km/s for the addopted value of $R_\odot$ in the present paper. Our solution has a an average slope

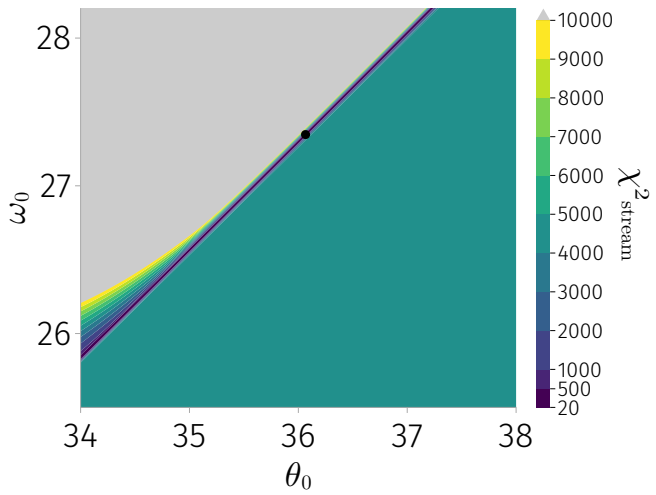

Fig. 3. $\chi^2_{\rm stream}$ function for $(\epsilon, \beta_0) = (56, 1.258 \times 10^{-5})$ in the window $(\theta_0, \omega_0) \in [34, 38] \times [25.5, 28.2]$. The black point corresponds to our fitted solution. It can be noticed that the minimum values of the function are located along a thin and finite *valley*.

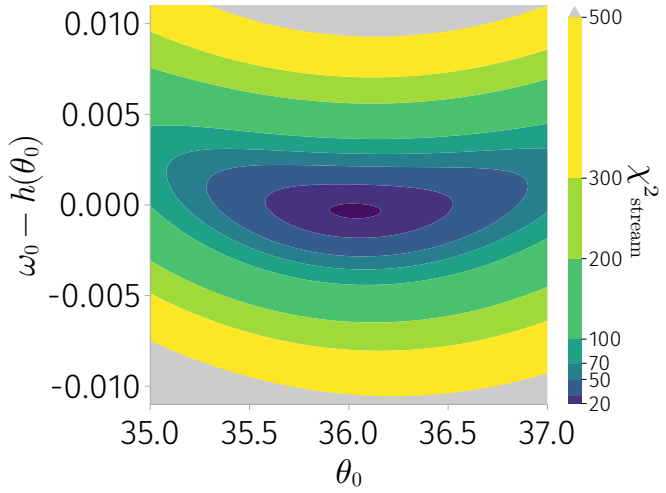

Fig. 4. $\chi^2_{\rm stream}$ function for $(\epsilon, \beta_0) = (56, 1.258 \times 10^{-5})$ in the window $(\theta_0, \omega_0 - h(\theta_0)) \in [35, 37] \times [-0.011, 0.011]$.

$s \approx -3.44$ km s^{-1} kpc^{-1}, fitted for Galactocentric distances between 5 and 40 kpc, which is a bit larger in magnitutude than the value of $s = -2.18$ km s^{-1} kpc^{-1} measured by Jiao et al. (2023).

Our dark matter solution has a finite (virial) radius of $r_{\rm DM,vir} = 27.4$ kpc and a virial mass of $m_{\rm DM,vir} = 1.4 \times 10^{11} M_\odot$. The total baryon mass of our model is approximately $m_b = 0.9 \times 10^{11} M_\odot$, implying that the total virial mass amounts to $m_{\rm vir} = 2.3 \times 10^{11} M_\odot$. The value of the MW total mass at 50 kpc reported in Table 3 of Gibbons et al. (2014) is $2.9 \times 10^{11} M_\odot$ with $(\sigma, 2\sigma) = (0.4, 0.9) \times 10^{11} M_\odot$, so our solution is contained in the 2σ region. It should be noted that as our solution's mass gets constant for radius larger $r_{\rm DM,vir}$ while the model studied by Gibbons et al. (2014) reaches larger estimated masses according to their Table 3. Nevetheless, their estimations at large radii have relatively high error bounds, e.g. $2\sigma = 3 \times 10^{11} M_\odot$ for $M(200{\rm kpc}) = 5.6 \times 10^{11} {\rm M}_\odot$. We would like to point out that there are recent model-dependent MW mass estimations performed by by Jiao et al. (2023) and Ou et al. (2023) which give even smaller values of the MW virial mass of approximately $1.99 \times 10^{11} M_\odot$ and $2.13 \times 10^{11} M_\odot$, respectively

Our fitted fermionic DM model has a density at the solar neighbourhood of $\rho_{DM,\odot} = 1.46 \times 10^7 M_\odot$ kpc^{-3} = 0.55 GeV cm^{-3}/c^2 which belongs to the 2σ region of the estimation made by Salucci, P. et al. (2010).

3.3. Varying the fermion mass to reach more compact cores

As already mentioned, we have found a solution that is in agreement with both GD-1 data and the geodesic motion of S2 and G2 at Sagittarious A*. But it is also true that any fermionic solution with a core mass $m_c \approx m_{\rm core}$ and more compact than our solution for $m = 56$ keV, will also satisfy the S-stars contraint. It is interesting to find out how much compactness can be reached while keeping simultaneously the S-stars and GD-1 contraints in the light of the new observations of the Event Horizon Telescope Collaboration (2022) which suggest a compactness of the order of magnitude of 5 Schwarzschild radii. A precise ray tracing study about simulated images of the central cores of fermionic distributions is on progress, trying to put strict constraints on the minimum compactness needed so as to be in agreement with the EHT observations. In order to extend our solutions to other values of the fermion mass (m), we used the second optimization algorithm described in Sec. 2.4 for $\epsilon = 100, 200, 300, 360$ keV. For each fermion mass we divided a given macroscopic orthohedron in parameter space in $20^3 = 8000$ smaller orthoedrons. Each subregion was optimized in a parallel distributed scheme, searching for those parameters that minimize $\chi^2_{\rm full}$ with the `NOMAD` algorithm. Afterwards, we selected the global minimum by comparing the results of each distributed process. The result is that for all the fermion masses it is possible to find values of the other parameters in such a way that the GD-1 stream is fitted with the same quality as the initial ($m = 56$) case. In fact, as will be shown in Fig. 6, all the solutions have the same density profile in the halo region, while their difference is limited to the compactness of the core.

4. Conclusions

We have fitted the GD-1 stream with an orbit in a MW potential built by a relativistic fermionic King DM distribution plus a set of fixed baryion distributions previously fitted by Pouliasis et al. The general procedure was to fix the value of the fermion mass while floating the other three fermionic parameters in order to fit simultaneously two astrophysical constraints: the stream observables and a DM core mass of $3.5 \times 10^6 M_\odot$, where the latter comes from previous fits of the S-star cluster at the centre of the Galaxy. This allowed us to reproduce with high accuracy, for fermion masses ranging from 56 to 360 keV, the polynomials fitted by Ibata et al. (2020) that correspond to sky position, proper motion, photometric distance and radial velocity measurements. Note that the core radius does not include all the core mass because it is defined as the radius in which the circular velocity reaches its first maximum corresponding to a distance in which the core density is still falling. We have fitted the stream track with a spherical fermionic DM distribution similarly to the fit performed by Malhan & Ibata (2019) with a triaxial generalization of the NFW distribution, obtaining agreement in both rotation curves at Galactocentric distances corresponding to the stream observables, i.e. $11.5 \leq D_g \leq 16.4$ (kpc). The slope of our Fermionic-MW model's rotation curve between 5 and 40 kpc is $s \approx -3.44$ km s^{-1} kpc^{-1}.

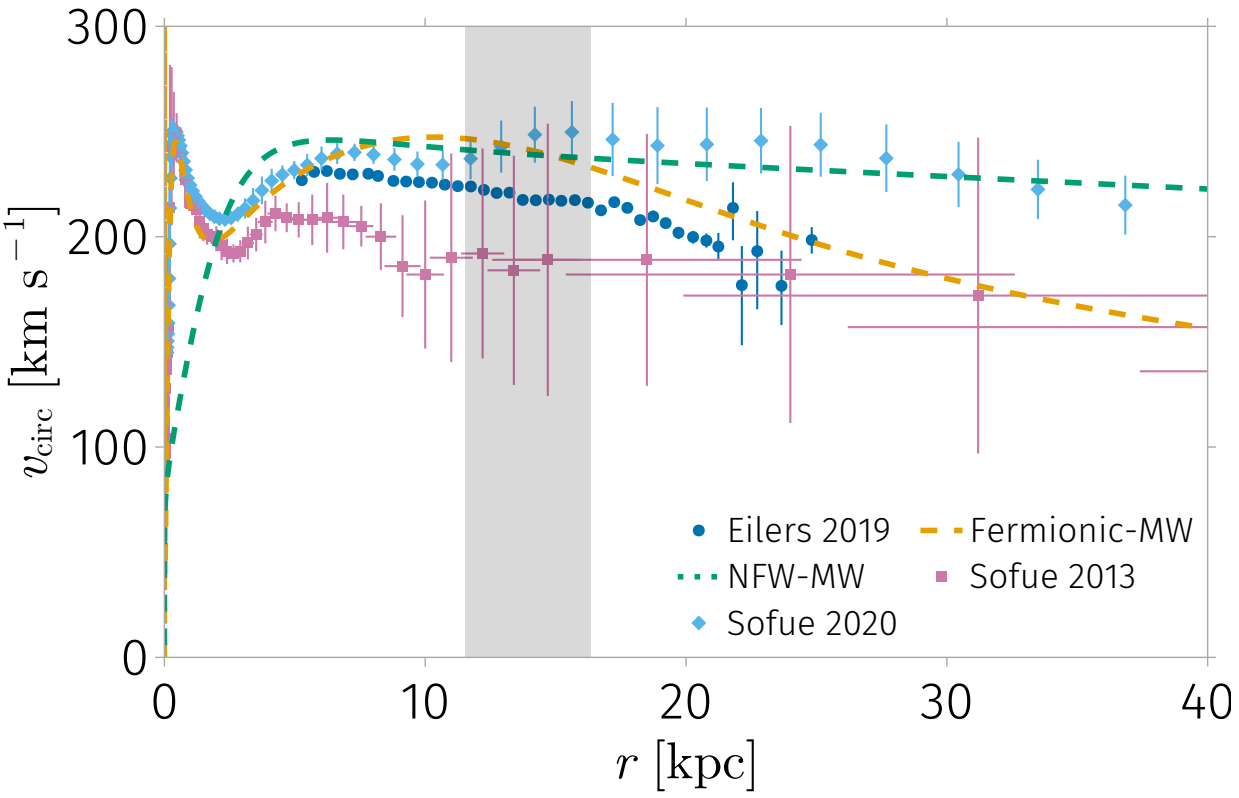

Fig. 5. Rotation curve of MW models and observations: NFW-MW model in dotted (green), Fermionic-MW in dashed (amber), Sofue (2013) with squares (magenta), Eilers et al. (2019) with circles (blue) for Eilers et al. (2019) and Sofue (2020) with rhombus (light-blue). The region where the GD-1 stream is located at cero redshift is displayed with a vertical grey band.

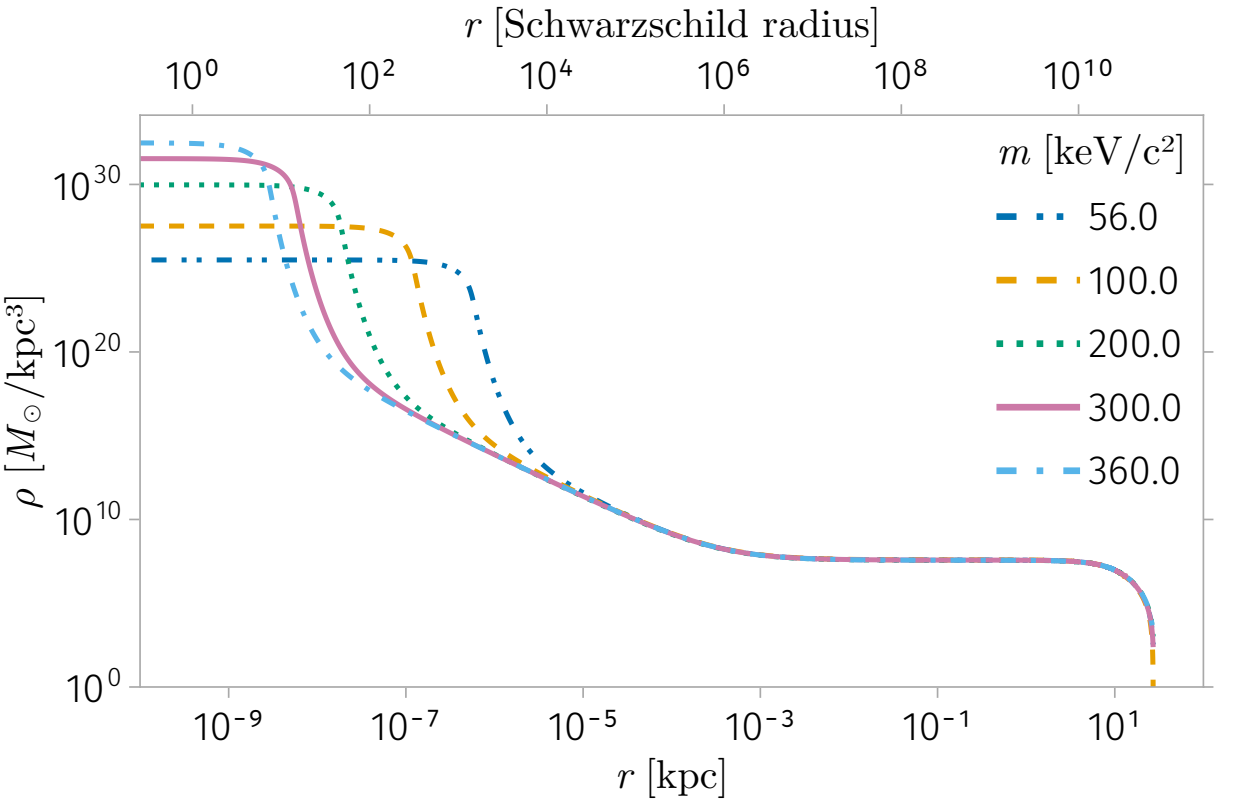

Fig. 6. Fermionic dark matter density profiles. The Schwarzschild radius was computed assuming a black hole mass of $m_{\rm bh} = 4.075 \times 10^6 M_\odot$.

We have found a circular velocity at the sun's position of $v_c(R_\odot) \approx 244$ km s^{-1} equal to the value obtained by Malhan & Ibata (2019). Our fermionic DM solution has a finite radius of $r_{\rm DM,vir} = 27.4$ kpc and virial mass of $m_{\rm DM,vir} = 1.4 \times 10^{11}\ M_\odot$, implying a total (DM+baryons) virial mass of the galaxy of $m_{\rm vir} = 2.4 \times 10^{11}\ M_\odot$, which is at a distance of 2σ from the value reported in Table 3 of Gibbons et al. (2014) for a radius of 50 kpc. The value obtained for the DM density at the solar neighbourhood is around $\rho_{DM,\odot} = 1.46 \times 10^7 M_\odot$ kpc^{-3} = 0.55 GeV cm^{-3}/c^2 which belongs to the 2σ region of a previos estimate (Salucci, P. et al. 2010). Finally, we have shown that it is possible to find a unidimensional family of solutions parametrized by the fermion mass, which have the same halo that fits the GD-1 stream but they differ in the compactness of the central core. For the limiting case studied here ($m = 360$ keV) we obtain a core radius of $r_c \approx 5$ Schwarzschild radii where the transformation to this distance unit was done assuming a black hole mass of $m_{\rm bh} = 4.075 \times 10^6$.

Acknowledgements. MFM thanks Khyati Malhan for his comments about the NFW-MW model. MFM thanks Leandro Martínez, Ian Weaver and the Julia community for their great support with the language and workflow. MFM thanks Juan Ignacio Rodriguez for his great support with hardware and software issues regarding the IALP server and personal computers. This work used computational resources from CCAD – Universidad Nacional de Córdoba (https://ccad.unc.edu.ar/), which are part of SNCAD – MinCyT, República Argentina. This work also used computational resources from the HPC center DIRAC, funded by Instituto de Física de Buenos Aires (UBA-CONICET) and part of SNCAD-MinCyT initiative, Argentina. The figures presented in this work where made with the *AlgebraOfGraphics.jl* (https://aog.makie.org/dev/) and *Makie.jl* (Danisch & Krumbiegel 2021) packages. Some of our optimization results were initially guided by the use of the `LN_NELDERMEAD` (Nelder & Mead 1965; Box 1965; Shere 1974) algorithm, from the *NLopt.jl* (Johnson 2007) package. In order to run Julia in a parallel SLURM environment we made use of the *Distributed.jl* and *SlurmClusterManager.jl* packages.

References

Amorisco, N. C. 2015, MNRAS, 450, 575
Argüelles, C. R., Krut, A., Rueda, J. A., & Ruffini, R. 2019, Physics of the Dark Universe, 24, 100278
Argüelles, C. R., Mestre, M. F., Becerra-Vergara, E. A., et al. 2022, MNRAS, 511, L35
Argüelles, C. R., Krut, A., Rueda, J. A., & Ruffini, R. 2018, Physics of the Dark Universe, 21
Astropy Collaboration, Price-Whelan, A. M., Lim, P. L., et al. 2022, apj, 935, 167
Astropy Collaboration, Price-Whelan, A. M., Sipőcz, B. M., et al. 2018, AJ, 156, 123
Astropy Collaboration, Robitaille, T. P., Tollerud, E. J., et al. 2013, A&A, 558, A33
Audet, C., Digabel, S. L., Montplaisir, V. R., & Tribes, C. 2021, NOMAD version 4: Nonlinear optimization with the MADS algorithm
Becerra-Vergara, E. A., Argüelles, C. R., Krut, A., Rueda, J. A., & Ruffini, R. 2020, A&A, 641, A34
Becerra-Vergara, E. A., Argüelles, C. R., Krut, A., Rueda, J. A., & Ruffini, R. 2021, MNRAS, 505, L64
Bezanson, J., Edelman, A., Karpinski, S., & Shah, V. B. 2017, SIAM review, 59, 65
Bovy, J. 2020, arXiv e-prints, arXiv:2012.02169
Box, M. J. 1965, The Computer Journal, 8, 42
Carlberg, R. G. 2018, ApJ, 861, 69
Chavanis, P.-H. 2020, European Physical Journal Plus, 135, 290
Collaboration, T. E. H. T. 2022, The Astrophysical Journal Letters, 930
Craig, P., Chakrabarti, S., Sanderson, R. E., & Nikakhtar, F. 2023, ApJ, 945, L32
Cunningham, E. C., Hunt, J. A. S., Price-Whelan, A. M., et al. 2023, arXiv e-prints, arXiv:2307.08730
Danisch, S. & Krumbiegel, J. 2021, Journal of Open Source Software, 6, 3349
de Boer, T. J. L., Belokurov, V., Koposov, S. E., et al. 2018, Monthly Notices of the Royal Astronomical Society, 477, 1893
Eilers, A.-C., Hogg, D. W., Rix, H.-W., & Ness, M. K. 2019, The Astrophysical Journal, 871, 120
Gialluca, M. T., Naidu, R. P., & Bonaca, A. 2021, ApJ, 911, L32
Gibbons, S. L. J., Belokurov, V., & Evans, N. W. 2014, MNRAS, 445, 3788
GRAVITY Collaboration, Abuter, R., Amorim, A., et al. 2018, A&A, 615, L15
Harris, C. R., Millman, K. J., van der Walt, S. J., et al. 2020, Nature, 585, 357
Helmi, A. 2020, ARA&A, 58, 205
Helmi, A., White, S. D. M., de Zeeuw, P. T., & Zhao, H. 1999, Nature, 402, 53
Ibata, R., Thomas, G., Famaey, B., et al. 2020, The Astrophysical Journal, 891, 161
Ibata, R. A., Lewis, G. F., & Martin, N. F. 2016, The Astrophysical Journal, 819, 1
Ibata, R. A., Lewis, G. F., Thomas, G., Martin, N. F., & Chapman, S. 2017, ApJ, 842, 120
Jiao, Y., Hammer, F., Wang, H., et al. 2023, arXiv e-prints, arXiv:2309.00048
Johnson, S. G. 2007, The NLopt nonlinear-optimization package, https://github.com/stevengj/nlopt
Johnston, K. V. & Carlberg, R. G. 2016, in Astrophysics and Space Science Library, Vol. 420, Tidal Streams in the Local Group and Beyond, ed. H. J. Newberg & J. L. Carlin, 169
Johnston, K. V., Zhao, H., Spergel, D. N., & Hernquist, L. 1999, ApJ, 512, L109
Klein, O. 1949, Rev. Mod. Phys., 21, 531
Koposov, S. E., Rix, H.-W., & Hogg, D. W. 2010, The Astrophysical Journal, 712, 260
Krut, A., Argüelles, C. R., Chavanis, P. H., Rueda, J. A., & Ruffini, R. 2023, ApJ, 945, 1
Law, D. R., Majewski, S. R., & Johnston, K. V. 2009, ApJ, 703, L67
Lux, H., Read, J. I., Lake, G., & Johnston, K. V. 2013, MNRAS, 436, 2386
Malhan, K. & Ibata, R. A. 2019, MNRAS, 486, 2995
Malhan, K., Ibata, R. A., Carlberg, R. G., Valluri, M., & Freese, K. 2019, ApJ, 881, 106
Malhan, K., Ibata, R. A., Goldman, B., et al. 2018, Monthly Notices of the Royal Astronomical Society, 478, 3862
Malhan, K., Valluri, M., & Freese, K. 2021, MNRAS, 501, 179
Merafina, M. & Ruffini, R. 1989, A&A, 221, 4
Mestre, M., Llinares, C., & Carpintero, D. D. 2020, MNRAS, 492, 4398
Nelder, J. A. & Mead, R. 1965, The Computer Journal, 7, 308
Nibauer, J., Belokurov, V., Cranmer, M., Goodman, J., & Ho, S. 2022, ApJ, 940, 22
Ou, X., Eilers, A.-C., Necib, L., & Frebel, A. 2023, arXiv e-prints, arXiv:2303.12838
Palau, C. G. & Miralda-Escudé, J. 2023, MNRAS, 524, 2124
Pouliasis, E., Di Matteo, P., & Haywood, M. 2017, A&A, 598, A66
Price-Whelan, A., Sipőcz, B., Lenz, D., et al. 2020, adrn/gala: v1.3
Price-Whelan, A. M. 2017, The Journal of Open Source Software, 2
Price-Whelan, A. M. & Bonaca, A. 2018, The Astrophysical Journal Letters, 863, L20
Price-Whelan, A. M., Johnston, K. V., Valluri, M., et al. 2016, MNRAS, 455, 1079
Qian, Y., Arshad, Y., & Bovy, J. 2022, MNRAS, 511, 2339
Ramos, P., Antoja, T., Yuan, Z., et al. 2022, A&A, 666, A64
Reino, S., Rossi, E. M., Sanderson, R. E., et al. 2021, MNRAS, 502, 4170
Salucci, P., Nesti, F., Gentile, G., & Frigerio Martins, C. 2010, A&A, 523, A83
Schönrich, R., Binney, J., & Dehnen, W. 2010, Monthly Notices of the Royal Astronomical Society, 403, 1829
Shere, K. 1974, Commun. ACM, 17, 471
Sofue, Y. 2013, Publications of the Astronomical Society of Japan, 65, 118
Sofue, Y. 2020, Galaxies, 8
Thomas, G. F., Famaey, B., Ibata, R., Lüghausen, F., & Kroupa, P. 2017, A&A, 603, A65
Tolman, R. C. 1930, Phys. Rev., 35, 904
Van Rossum, G. & Drake Jr, F. L. 1995, Python tutorial (Centrum voor Wiskunde en Informatica Amsterdam, The Netherlands)
Vera-Ciro, C. & Helmi, A. 2013, ApJ, 773, L4
Virtanen, P., Gommers, R., Oliphant, T. E., et al. 2020, Nature Methods, 17, 261
Zhao, H., Johnston, K. V., Hernquist, L., & Spergel, D. N. 1999, A&A, 348, L49